

# Transitions from nanoscale to microscale dynamic friction mechanisms on polyethylene and silicon surfaces

S. Niederberger and D. H. Gracias

*Department of Chemistry, University of California, Berkeley, California 94720 and Materials Science Division, Lawrence Berkeley National Laboratory, Berkeley, California 94720*

K. Komvopoulos<sup>a)</sup>

*Department of Mechanical Engineering, University of California, Berkeley, California 94720*

G. A. Somorjai

*Department of Chemistry, University of California, Berkeley, California 94720 and Materials Science Division, Lawrence Berkeley National Laboratory, Berkeley, California 94720*

(Received 21 May 1999; accepted for publication 24 November 1999)

The dynamic friction mechanisms of polyethylene and silicon were investigated for apparent contact pressures and contact areas in the ranges of 8 MPa–18 GPa and 17 nm<sup>2</sup>–9500 μm<sup>2</sup>, respectively. Friction force measurements were obtained with a friction force microscope, scanning force microscope, and pin-on-disk tribometer. Silicon and diamond tips with a nominal radius of curvature between 100 nm and 1.2 mm were slid against low- and high-density polyethylene and Si(100) substrates under contact loads in the range of 5 nN–0.27 N. The low friction coefficients obtained with all material systems at low contact pressures indicated that deformation at the sliding interface was primarily elastic. Alternatively, the significantly higher friction coefficients at higher contact pressures suggested that plastic deformation was the principal mode of deformation. The high friction coefficients of polyethylene observed with large apparent contact areas are interpreted in terms of the microstructure evolution involving the rearrangement of crystalline regions (lamellae) nearly parallel to the sliding direction, which reduces the surface resistance to plastic shearing. Such differences in the friction behavior of polyethylene resulting from stress-induced microstructural changes were found to occur over a relatively large range of the apparent contact area. The friction behavior of silicon was strongly affected by the presence of a native oxide film. Results are presented to demonstrate the effect of the scale of deformation at the contact interface on the dynamic friction behavior and the significance of contact parameters on the friction measurements obtained with different instruments. © 2000 American Institute of Physics. [S0021-8979(00)06305-2]

## I. INTRODUCTION

Friction force measurements can be obtained with various instruments, such as friction force microscope (FFM),<sup>1–3</sup> scanning force microscope (SFM),<sup>4,5</sup> and classical pin-on-disk (POD) tribometer.<sup>6</sup> All of these instruments operate in totally different load and contact area regimes. The main objective in FFM studies has been the examination of local friction properties,<sup>3,7</sup> whereas the focus in investigations using the POD has been the study of the evolution of wear,<sup>8,9</sup> the analysis of the effects of operating conditions,<sup>9–11</sup> and the role of blends and additives on the tribological properties.<sup>8,12</sup> The FFM is used to apply loads in the nanoNewton range with silicon or silicon nitride tips with a radius of curvature of 20–100 nm. This instrument is the workhorse of nanotribology, a rapidly growing field dealing with tribology science and technology problems encountered at the nanoscale. The SFM is a modified FFM that uses diamond tips of intermediate radius of curvature (typically from about 50 nm up to 20 μm) and is capable of applying loads in the microNewton range. This instrument is well suited to bridge the

gap between nanotribology and traditional tribology. Finally, the POD can be used with a variety of tips, with blunt spherical pins having a radius of curvature of the order of a few millimeters being the most common. Although sensitive POD instruments can apply loads in the milliNewton range, loads of the order of 1 N or higher can be applied with more rigid POD instruments.

The ranges of normal load and contact area obtained with the above-mentioned instruments may yield different types of interactions between contacting surfaces. Specifically, at very low contact pressures elastic forces are dominant and surface adhesion plays a significant role. Alternatively, at high contact pressures the hard tip penetrates the flat sample surface and, thus, the contribution of the plowing friction mechanism to the overall friction increases.<sup>6,13,14</sup> Microprobe instruments provide the means for distinguishing differences in surface properties at scales of several micrometers down to atomic dimensions. Due to the profoundly different material behavior at submicron scales, tribological properties measured with microprobe instruments (e.g., FFM) may differ significantly from those obtained with traditional equipment that cause deformation over a much

<sup>a)</sup>Electronic mail: kyriakos@euler.berkeley.edu

TABLE I. Properties of polymer samples.<sup>a</sup>

Property	Polymer material	
	LDP	HDP
Density (g/cm <sup>3</sup> )	0.92	0.95
Melting temperature (°C)	115	131
Molecular weight (g/mol)	...	125×10 <sup>3</sup>
Crystallinity <sup>b</sup> (%)	~23	~65

<sup>a</sup>See Ref. 15.<sup>b</sup>Determined by measuring heats of fusion after molding of the samples using differential scanning calorimetry.

larger volume of the test specimen (e.g., POD). In addition, the transition from nanoscopic to microscopic deformation may promote the dominance of different mechanisms, depending on the microstructure sensitivity of the material (e.g., pressure dependence of shear strength of polymeric materials) on the resulting contact conditions (i.e., contact pressure and real contact area). Hence, the objectives of the present investigation were to perform friction experiments on low-density polyethylene (LDP), high-density polyethylene (HDP), and silicon with all three instruments (FFM, SFM, and POD) using loads and apparent contact areas varying by approximately eight orders of magnitude. Another purpose of this study was to analyze the results obtained in totally different load ranges and to investigate possible trends that may have predictive value.

## II. EXPERIMENTAL PROCEDURES

### A. Specimen preparation

In order to avoid the effect of topography variations on the friction measurements, pure granulates of low- and high-density polyethylene (Aldrich Chemical Co.) were melted and pressed against a smooth glass plate for an hour to produce flat disk specimens with smooth surfaces. The polymer specimens were cooled to room temperature in about 20 min. Table I gives some important properties of the produced polymers.<sup>15</sup> Round disks of about 1.27 cm in diameter were cut from commercially available Si(100) wafers. From 10  $\mu\text{m} \times 10 \mu\text{m}$  surface area images, the rms roughness of the polyethylene and silicon disks was found equal to 30 and 4 nm, respectively. Apart from significant interest on the nano- and microtribological properties of silicon (the main structural material in microelectronics), the microstructure of silicon is insensitive to contact pressure variations. Therefore, it can be used as a reference material to study whether transitions in the friction behavior of polymers due to pressure-induced microstructure changes can be probed with the instruments used in this study. In view of profound differences in the microstructure and mechanical properties of polyethylene and silicon, increasing the contact load (or mean contact pressure and apparent contact area) may yield remarkably different sliding friction mechanisms.

## B. Instrumentation and testing techniques

### 1. Friction force microscope

A commercially available friction force microscope (FFM) (Park Scientific Instruments, Autoprobe MN5) was used to perform friction testing at the nanoscale. A laser and a position-sensitive photodiode were used to determine the tip deflection during surface probing. Friction was measured by obtaining line scans at several predetermined repulsive loads. Silicon probes of different spring constants and tip radius equal to 150 and 200 nm were used to apply normal loads in the range of 5–700 nN. The sliding speed in all the FFM tests was fixed at 520 nm/s. The tip radius was estimated by scanning each tip over the very sharp wedges of a strontium titanate (SrTiO<sub>3</sub>) surface. Since the produced traces were self-images of the scanning tips, the tip radii of curvature were found by fitting a parabola to the apex of each feature. To determine the magnitude of the friction force, the FFM was calibrated for each tip according to the technique of Ogletree, Carpick, and Salmeron.<sup>16</sup> The dependence of the lateral signal on the vertical signal was determined from friction and topographic images obtained on two well-defined tilted planes [the (101) and (103) planes of SrTiO<sub>3</sub>] at different loads. Calibration of the friction force for tips with radius of curvature equal to about 150 and 200 nm involves some error because this method is ideal for much smaller tips having a radius of curvature equal to ~50 nm. This error was taken into account in the calculation of the friction data.

### 2. Scanning force microscope

Friction testing at the microscale was performed with a scanning force microscope<sup>5</sup> (SFM) consisting of an atomic force microscope (Digital Instruments, Nanoscope II) retrofitted with a capacitive force transducer (Triboscope, Hysitron Inc.). The vertical and lateral (friction) forces were determined by two independent capacitor plates that were previously calibrated for each tip. A detailed description of the SFM tip calibration procedure can be found elsewhere.<sup>5</sup> Friction testing at the microscale was performed by sliding a 90° three-sided pyramidal diamond tip or a 60° conical diamond tip with radii of curvature equal to 100 nm and 16  $\mu\text{m}$ , respectively, on the disk surfaces at a constant speed of 400 nm/s and loads in the range of 2–1000  $\mu\text{N}$ .

### 3. Pin-on-disk apparatus

Friction testing at the millimeter scale was performed with a pin-on-disk (POD) apparatus. A cantilever beam holding a pin with a blunt, diamond-coated tip of radius 1.2 mm was wired with four strain gauges in a Wheatstone bridge configuration. The normal force (in the range of 17–270 mN) was applied directly to the pin as a dead weight, and the friction force was measured by the strain gauges. A deflection constant of 12.3 mN/V was determined from several calibration measurements. The strain-gauge output voltage was passed through an amplifier and was subsequently collected by a data acquisition system. The sliding speed in all the POD tests was fixed at 4.2 mm/s. Friction coefficient data were recorded continuously at a rate of 1.5 Hz.

TABLE II. Testing parameters for different instruments.

Instrument	Sliding speed	Sliding tip	Normal load
FFM	520 nm/s	Silicon (radius=150 nm)	5–20 nN
		Silicon (radius=200 nm)	20–700 nN
SFM	400 nm/s	Diamond (radius=100 nm)	2–100 $\mu$ N
		Diamond (radius=16 $\mu$ m)	2–1000 $\mu$ N
POD	4.2 mm/s	Diamond (radius=1.2 mm)	27–270 mN

The experimental parameters for each instrument are given in Table II. All the experiments were performed in a clean-air laboratory environment at room temperature and relative humidity of approximately 40%.

#### 4. Surface imaging

To determine the prevailing deformation mode at the tip–substrate interface, disk surface images were obtained before and after testing with each instrument. Since the FFM and SFM have both scratching and *in situ* imaging capabilities, surface imaging was performed with the same tip directly after testing at much lighter loads (of the order of a few nanoNewtons). The wear tracks generated by the POD tester were examined with an optical microscope.

### III. RESULTS AND DISCUSSION

The apparent contact area and corresponding mean contact pressure were determined in terms of the tip radius, applied normal load, and elastic properties of the surfaces using the classical Hertz theory.<sup>17</sup> The elastic modulus of LDP and HDP was assumed to be equal to 0.6 and 0.9 GPa, respectively,<sup>18</sup> and that of Si(100) equal to 98 GPa. A Poisson's ratio of 0.3 was assumed for all materials. Where the penetration depth was sufficiently large for the contact area to be affected by the global tip geometry (e.g., SFM pyramidal and conical tips), the apparent contact pressure was de-

termined by dividing the normal load by the projected contact area, obtained from the tip geometry and measured wear track depth. The steady-state dynamic friction coefficients of all material systems are given in Table III in terms of ranges of applied normal load and calculated apparent contact area and mean contact pressure.

Figure 1 shows the steady-state friction force as a function of normal load for LDP obtained from sliding experiments performed with different instruments. Within each load range, all measurements reveal a linear dependence of the friction force on normal load. Since the ratio of the friction force to the normal load is, by definition, equal to the coefficient of friction  $\mu$ , the slope of the lines fitted through the data shown in Fig. 1 (as well as in subsequent similar figures) represent the steady-state friction coefficient in each load range. A transition in the coefficient of friction within a load range is reflected by the change of the slope of the fitted line. Assuming that a similar coefficient of friction is an indication of the same active friction mechanism and that a significant change in the coefficient of friction is due to the occurrence of different mechanism(s), three distinct friction regimes can be identified in Fig. 1. The low-load range of the FFM results [Fig. 1(a)] shows a very low coefficient of friction ( $\mu \approx 0.06$ ). The high-load range of the FFM results beginning at  $\sim 200$  nN [Fig. 1(a)] and the results obtained with SFM tips of radius of curvature equal to 100 nm and 16  $\mu$ m [Figs. 1(b) and 1(c), respectively] and contact loads appreciably higher than those in the FFM tests reveal much higher friction coefficients ( $\mu \approx 0.13$ – $0.18$ ). A remarkably higher friction coefficient ( $\mu \approx 0.41$ ) was observed in the POD experiments with significantly higher contact loads [Fig. 1(d)] that resulted in much larger apparent contact areas.

Figure 1 and Table III show that the coefficient of friction is strongly affected by the magnitudes of the applied normal load and apparent contact area. The transition in friction observed in Fig. 1(a) occurs at a load of  $\sim 200$  nN, corresponding to a mean contact pressure of 70 MPa. To further study the observed transition, LDP surfaces were imaged with the FFM before and after testing at much lighter

TABLE III. Friction coefficients of high- and low-density polyethylene and silicon vs normal load, apparent contact area, and mean contact pressure obtained with different instruments.

Material	Instrument	Normal load	Apparent contact area	Mean contact pressure	Friction coefficient
LDP	FFM	5–200 nN	200–2800 nm <sup>2</sup>	25–70 MPa	0.06
		200–700 nN	2800–6700 nm <sup>2</sup>	70–105 MPa	0.17
	SFM	2–80 $\mu$ N	1300 nm <sup>2</sup> –1.9 $\mu$ m <sup>2</sup>	42–1625 MPa	0.18
		2–1000 $\mu$ N	0.25–15 $\mu$ m <sup>2</sup>	8–67 MPa	0.13
HDP	POD	17–85 mN	1900–5300 $\mu$ m <sup>2</sup>	9–16 MPa	0.41
		5–200 nN	200–2800 nm <sup>2</sup>	25–70 MPa	0.06
	SFM	200–700 nN	2800–6700 nm <sup>2</sup>	70–105 MPa	0.13
		2–30 $\mu$ N	260 nm <sup>2</sup> –0.059 $\mu$ m <sup>2</sup>	0.51–7.7 GPa	0.20
Si	FFM	30–80 $\mu$ N	0.059–0.42 $\mu$ m <sup>2</sup>	0.19–0.51 GPa	0.39
		2–1000 $\mu$ N	0.25–15 $\mu$ m <sup>2</sup>	8–67 MPa	0.11
	POD	17–210 mN	1900–9500 $\mu$ m <sup>2</sup>	9–22 MPa	0.17
		5–700 nN	17–450 nm <sup>2</sup>	0.3–1.54 GPa	0.03
SFM	10–70 $\mu$ N	1060–3900 nm <sup>2</sup>	9.4–18 GPa	0.25	
	2–1000 $\mu$ N	0.011–0.66 $\mu$ m <sup>2</sup>	0.19–1.51 GPa	0.11	
POD	17–270 mN	81–500 $\mu$ m <sup>2</sup>	210–540 MPa	0.08	

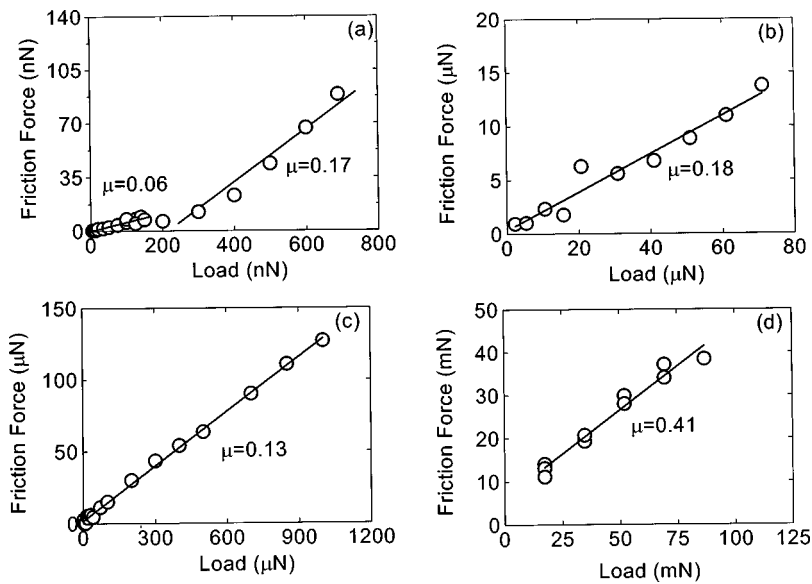


FIG. 1. Friction force vs load for LDP obtained with (a) FFM (150 nm tip radius), (b) SFM (100 nm tip radius), (c) SFM (16  $\mu\text{m}$  tip radius), and (d) POD (1.2 mm pin radius).

loads in order to examine the surface condition. Since changes in the surface topography after sliding under normal loads less than 200 nN could not be revealed, at least within the instrument resolution, it may be argued that in this range of contact loads (i.e., pressure range of 25–70 MPa) the deformation of LDP was essentially elastic. Consequently, the low friction in this regime is considered to be a manifestation of surface adhesion forces and roughness effects. The very shallow scratches produced on LDP surfaces at loads greater than 200 nN indicated that plastic deformation was dominant and that the higher friction in this regime was mainly due to plowing and microcutting processes occurring at the nanometer scale. FFM surface images obtained before and after scratching the LDP surfaces with the same tip under a load of 700 nN confirmed the formation of shallow plowing grooves.

The fact that a transition in friction is not shown in Figs. 1(b) and 1(c) and the corresponding friction coefficients are similar to that of the high-friction regime in Fig. 1(a) suggests that plastic deformation was mainly due to plowing and cutting processes occurring at the nanometer and micrometer scales. To ensure that plasticity was significant in the load range of 2–1000  $\mu\text{N}$ , indentations were performed with the

SFM instrument using a  $90^\circ$  three-sided pyramidal diamond tip of radius  $\sim 100$  nm and maximum load ranges similar to those in Figs. 1(b) and 1(c). Figure 2 shows three representative indentation curves from these experiments for a maximum normal load approximately equal to 5, 12, and 27  $\mu\text{N}$ . The force hysteresis and residual penetration depths shown in Fig. 2 indicate that plastic deformation occurred even with loads as low as 5  $\mu\text{N}$ . The good agreement between the three loading paths illustrates the instrument's capability to reliably probe the mechanical behavior of LDP. Unloading produces a highly nonlinear force response characteristic of a viscoelastic material. The results shown in Fig. 2 confirm that significant plastic deformation occurred even in the light-load range of Figs. 1(b) and 1(c). It should be noted that because the geometry of the SFM tip is pyramidal or conical, the produced contact pressures are higher than those obtained with spherical tips of the same radius of curvature. Surface topography images obtained after friction testing provided additional evidence for the occurrence of plastic deformation. Figure 3 shows an image of a wear groove on a LDP surface generated by sliding a 150 nm radius FFM silicon tip under a mean contact pressure of  $\sim 150$  MPa. The

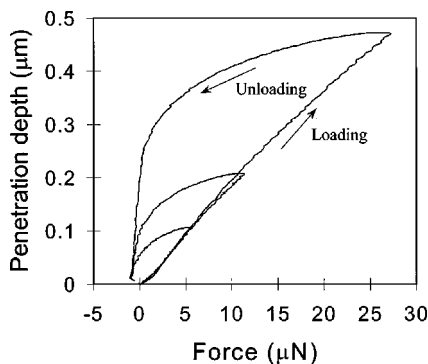


FIG. 2. Indentation force vs penetration depth curves for LDP obtained with a  $90^\circ$  three-sided pyramidal diamond SFM tip having a radius of curvature equal to 100 nm for a maximum indentation load of about 5, 12, and 27  $\mu\text{N}$ .

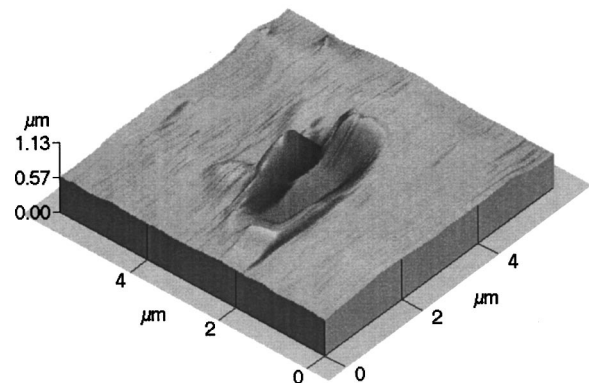


FIG. 3. Wear scar on a LDP surface produced by sliding a FFM silicon tip of radius of curvature equal to 150 nm under a mean contact pressure of about 150 MPa.

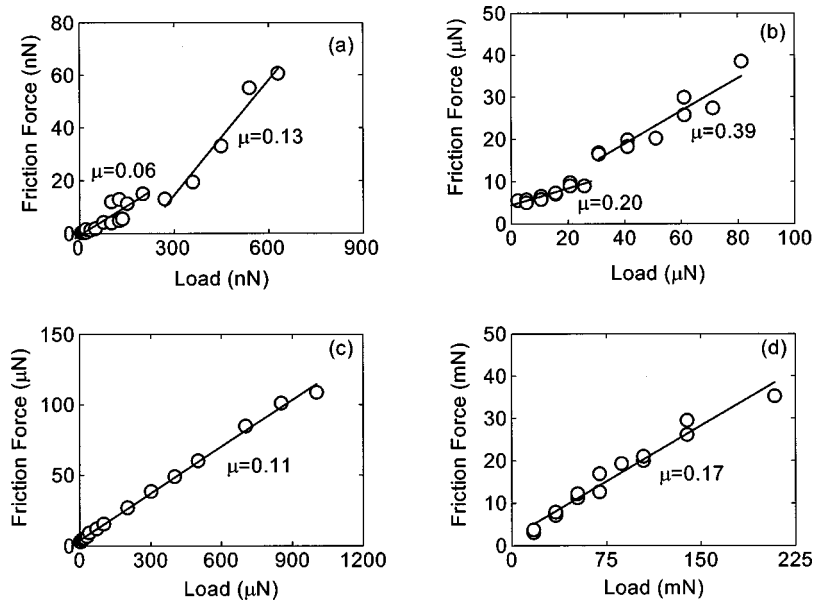


FIG. 4. Friction force vs load for HDP obtained with (a) FFM (150 nm tip radius), (b) SFM (100 nm tip radius), (c) SFM (16  $\mu$ m tip radius), and (d) POD (1.2 mm pin radius).

groove length corresponds to the duration of sliding between the loading and unloading operations.

From the penetration depths in the SFM experiments, it is apparent that the real contact area and plastic flow behavior were mostly affected by the overall tip shape rather than its radius of curvature. The specific SFM tip shape and the approximately linear dependence of load on penetration depth (due to the occurrence of plastic deformation) yield a pressure proportional to the reciprocal of the applied load, which is different from the other setups where the pressure increases with the normal load due to the different contact geometry. Thus, a higher pressure was produced in the low-load SFM tests (Table III). Considering the approximately linear loading paths shown in Fig. 2 and the dependence of the resulting mean pressure on the SFM tip shape, it may be interpreted that the mean contact pressure in the tests performed with the sharper tip [Fig. 1(b)] was higher than that in the tests involving the relatively blunt tip [Fig. 1(c)] and, presumably, it was of the same order of magnitude with that in the FFM experiments [Fig. 1(a)]. This view is also supported by the similar values of the friction coefficient in Fig. 1(b) and the high-friction regime in Fig. 1(a), and the slightly lower friction produced with the blunt tip [Fig. 1(c)]. The latter may be associated with the relatively smaller penetration depths yielding a less contributing plowing friction mechanism,<sup>6,13,14</sup> and the reduced surface resistance against plowing and adhesive shearing due to the decrease of the strength of LDP with decreasing pressure.<sup>15</sup>

Figure 4 shows friction results for HDP obtained with different instruments. As with LDP, all measurements show linearity between friction force and normal load within a given load range. Figure 4(a) shows a transition from relatively low ( $\mu \approx 0.06$ ) to high ( $\mu \approx 0.13$ ) coefficient of friction, similar to what was observed with LDP at a load of  $\sim 200$  nN [Fig. 1(a)]. The experimental results obtained with the sharp SFM tip reveal a second transition in the friction behavior of HDP at a load of  $\sim 30$   $\mu$ N. Figure 4(b) shows that although the coefficient of friction in the load range of 2–30

$\mu$ N is similar to that of Fig. 1(b) a significantly higher coefficient of friction ( $\mu \approx 0.39$ ) was obtained at loads greater than 30  $\mu$ N. Despite the higher loads used in the SFM tests performed with the relatively blunt tip [Fig. 4(c)], a remarkably lower friction coefficient was produced ( $\mu \approx 0.11$ ). Significant differences in the friction behavior of HDP and LDP were observed in the POD experiments. A comparison of Figs. 1(d) and 4(d) indicates that HDP yields much lower friction coefficients ( $\mu \approx 0.17$ ) in the load range of 17–210 mN.

Although the FFM experiments showed a transition very similar to that of LDP, a relatively lower coefficient of friction was obtained with HDP at loads greater than 200 nN [Fig. 4(a)]. In view of the similarity of the FFM results shown in Figs. 1(a) and 4(a), it may be inferred that the dominant nanoscale friction mechanisms of HDP are the same as those of LDP. The transition in friction observed in the SFM experiments with the sharp tip and a load of  $\sim 30$   $\mu$ N [Fig. 4(b)] may be associated with the enhancement of plowing due to the greater penetration depths produced at higher loads. Considering the inverse dependence of pressure on normal load in the SFM tests discussed previously, it may be interpreted that the low friction in the low-load/high-pressure range is due to surface plowing, whereas the higher friction in the high-load/low-pressure range is indicative of the bulk friction behavior [Fig. 4(b)]. This is supported by the results presented in Fig. 4(c) for the relatively blunt tip where a much lower friction coefficient was produced despite the higher loads used in these tests. The contact pressure in Fig. 4(c) is in the range of the FFM measurements (Table III), and the friction coefficient is close to that corresponding to the high-friction regime in Fig. 4(a).

The results shown in Fig. 4 demonstrate a pronounced difference between surface and bulk friction properties. Since HDP is more susceptible to oxidation than LDP, it is likely that the friction behavior observed with the FFM and the SFM with the blunt tip [i.e., pressure range of 8–105 MPa (Table III)] was affected by the presence of an oxide

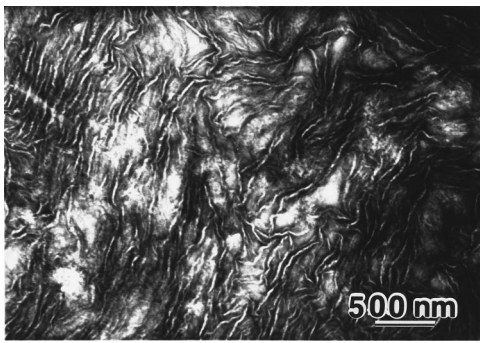


FIG. 5. Cross-section TEM micrograph of HDP obtained after sliding in the POD tester under a mean contact pressure of about 59 MPa.

layer, whereas the results obtained with the sharp SFM tip, especially at high loads in the range of 30–80  $\mu\text{N}$  (i.e., pressure range of 0.19–0.51 GPa) and the POD tester (i.e., large apparent contact area) are due to the combined effects of the surface and bulk friction behaviors. It is apparent, therefore, that in order to isolate the effect of the crystalline phase in HDP on the tribological behavior, surface oxidation during sample preparation must be controlled.

Even though the apparent contact pressure in the POD tests of LDP and HDP was relatively low (Table III), microscopy studies showed that plastic flow was the dominant deformation process. These observations suggest that, apart from asperities plowing through the material due to the locally higher contact pressures, an additional friction mechanism was also operative. It has been reported that the sliding process promotes the reorientation of crystalline platelets (lamella) in polyethylene parallel to the direction of sliding, thus reducing the shear strength of the polymer surface.<sup>14,19,20</sup> Because the typical lamella size is 50 nm or less, it is not likely that the very sharp tips (i.e., radius of curvature equal to 150 and 200 nm) used in the FFM and SFM instruments induced lamella alignment. However, a much blunter tip yields a significantly larger real contact

area, which promotes the process of lamella alignment. Figure 5 shows a representative cross-section transmission electron microscopy (TEM) micrograph of HDP obtained after sliding in the POD tester under a mean contact pressure of  $\sim 59$  MPa. A remarkable lamellae alignment almost parallel to the direction of sliding occurred to a depth of several nanometers below the sliding interface. Thus, the dominant friction mechanisms in the POD experiments were the plowing and cutting of the LDP and HDP surfaces by the harder asperities on the diamond-coated pin surface and wear particles trapped at the contact interface,<sup>6,13,14</sup> accompanied by plastic shearing adjacent to the sliding interface leading to lamellae alignment which, in turn, reduced the polymer surface resistance to plastic shearing.<sup>19,20</sup>

Results demonstrating the effect of the normal load and apparent contact pressure on the friction behavior of silicon are presented in Fig. 6 and Table III. Three distinct friction regimes with significantly different coefficients of friction can be observed. The FFM measurements show a very low coefficient of friction ( $\mu \approx 0.03$ ) throughout the entire load range [Fig. 6(a)]. A significantly higher coefficient of friction ( $\mu \approx 0.25$ ) was found in the SFM experiments with a tip of 100 nm radius [Fig. 6(b)]. However, in the SFM experiments with the relatively blunt tip of 16  $\mu\text{m}$  in radius of curvature [Fig. 6(c)] the coefficient of friction was much lower ( $\mu \approx 0.11$ ). A low friction coefficient ( $\mu \approx 0.08$ ) was also found in the POD experiments performed with the very blunt diamond-coated pin [Fig. 6(d)].

Despite the appreciably high contact pressures in the FFM experiments [in the range of 0.3–1.54 GPa (Table III)], a transition from elastic to plastic deformation did not occur in the load range 5–700 nN because silicon is much harder than polyethylene. Surface imaging of silicon surfaces tested with the FFM did not reveal any discernible changes in the surface topography due to sliding, confirming the absence of plowing scratches. The very low coefficient of friction obtained throughout this load range [Fig. 6(a)] is attributed to

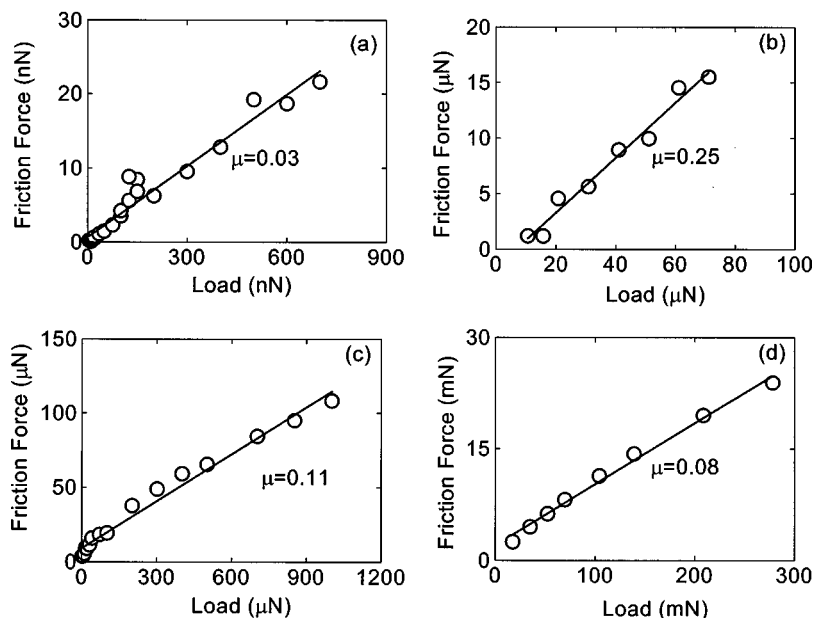


FIG. 6. Friction force vs load for Si(100) obtained with (a) FFM (150 nm tip radius), (b) SFM (100 nm tip radius), (c) SFM (16  $\mu\text{m}$  tip radius), and (d) POD (1.2 mm pin radius).

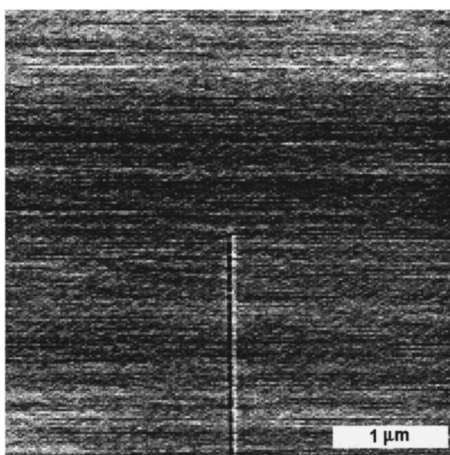


FIG. 7. AFM image showing a shallow scratch on a smooth Si(100) substrate produced by sliding a 100 nm radius SFM diamond tip under a load of  $70 \mu\text{N}$ .

the presence of a low surface energy, thin oxide film and the negligible roughness effect due to the smoothness of the silicon substrate. However, Fig. 6(b) shows that a significantly higher friction coefficient was produced with the sharp SFM tip at loads ranging from 10 to  $70 \mu\text{N}$ , i.e., mean contact pressures between 9.4 and 18 GPa (Table III). Surface imaging with the same tip at very light loads (of the order of  $0.5 \mu\text{N}$ ) produced conclusive evidence about the dominant role of plowing under these contact conditions. Figure 7 shows a characteristic atomic force microscope (AFM) image of a plowing groove generated on a silicon surface by sliding a 100 nm radius diamond tip under a load of  $70 \mu\text{N}$ . Since the measured groove depth is  $\sim 1$  nm, it may be concluded that plowing occurred within the oxide film. Thus, the primary friction mechanism in the 9.4–18 GPa pressure range is the plowing of the native oxide film on the silicon surface. Figure 6(c) shows that an appreciably lower friction coefficient was obtained with the blunt SFM tip at loads ranging from 2 to  $1000 \mu\text{N}$ , i.e., 0.19–1.51 GPa (Table III), apparently because of the less severe plowing effect at lower contact pressures. However, the fact that the friction coefficient is not as low as in Fig. 6(a) suggests that the work dissipated due to plowing through the oxide film is greater than that due to surface adhesion. Compared to polyethylene, much lower friction was obtained in the POD experiments [Fig. 6(d)]. This is again attributed to the dominance of surface adhesion and the minimal contribution of plowing due to the significantly lower contact pressures [i.e., 210–540 MPa (Table III)] and the higher yield strength of silicon.

In summary, the FFM yields the lowest coefficients of friction for all three materials. This is attributed to the predominantly elastic deformation dominating the friction process. However, above a critical load, wear-dominated friction and a profound increase of the coefficient of friction were observed. Even at light loads the contact pressure produced with the sharp tips in the FFM tests can be extremely high. Increasing the load in the SFM and POD experiments promoted the occurrence of wear processes and the simultaneous increase of the coefficient of friction. Both LDP and HDP not only exhibited pressure-controlled friction transi-

tions, but also transitions associated with the microstructure evolution during sliding, observed only with relatively large apparent contact areas. The average lamellae size of polyethylene is dictated by crystallization thermodynamics and is approximately 20–50 nm, depending on the processing temperature, pressure, and level of undercooling. Hence, the profound role of lamellae alignment parallel to the direction of sliding can only occur with relatively blunt tips producing contact areas significantly larger than the lamellae average size. The results shown in Figs. 1, 4, and 5 provide evidence for the effect of stress-induced lamellae alignment on the dynamic friction characteristics of polyethylene. Thus, a significant change in the friction behavior can occur, even for contact pressures of similar order of magnitude, by increasing the apparent contact area. This is supported by the friction results for LDP and HDP obtained from the SFM and POD tests for contact pressures in the range of 8–67 MPa (Table III). In addition, increasing the contact load without changing appreciably the real contact area leads to a transition from elastic to plastic surface deformation characterized by the dominance of surface adhesion and plowing friction mechanisms, respectively.

The results for silicon do not show a dependence of friction on contact area. This is expected because silicon possesses a very different microstructure. However, a transition from elastic to plastic deformation accompanied by a change from adhesion to plowing friction mechanisms was observed at contact pressures sufficiently high to cause rupture of the native oxide film. A second transition occurred when the pressure at asperity microcontacts was further increased to the point of promoting plowing of bulk silicon.

This study demonstrated the sufficient sensitivity of the instruments used to probe the dependence of dynamic friction on the dominant deformation mode and near-surface microstructure changes at normal loads and apparent contact areas varying by several orders of magnitude. The relatively small differences in the friction coefficients of LDP and HDP obtained with silicon and diamond tips indicate that the effects of the surface chemistry and mechanical properties of the two tips were secondary. Thus, the friction process was dominated by the polymer deformation and was independent of the chemical nature of the rigid tips. Future studies will concentrate on the characterization of polyethylene and silicon surfaces before and after testing to obtain detailed information about the near-surface microstructure and chemical state in order to further elucidate the variation of friction over a wide range of loads and contact areas.

#### IV. CONCLUSIONS

An experimental investigation of the dynamic friction behavior of LDP, HDP, and Si(100) was performed with different instruments at normal loads in the range of 5 nN–0.27 N. All materials revealed different friction regimes. A transition from elastic to plastic deformation accompanied by a change of the dominant friction mechanism from adhesion to plowing was observed with increasing load (or contact pressure) in all tests. In addition, a dependence of friction on the apparent contact area was found for polyethylene. This

was associated with the strong effect of pressure on the shear strength of polyethylene and the modification of the microstructure adjacent to the sliding interface through the alignment of microcrystalline phases (lamellae) parallel to the sliding direction. The lamellae alignment reduces the shear strength of the polymer surface and, hence, increases the contribution of the plowing friction mechanism to the overall friction. Such a change of the polymer microstructure was not observed with relatively sharp tips producing real contact areas of the order of the average lamellae size or less. Contrary to LDP, the coefficient of friction of HDP was found to strongly depend on the scratch depth, presumably due to the presence of a slightly oxidized surface layer. Although silicon did not show a structure-sensitive friction behavior, a dependence of friction on scratch depth was also observed and was related to the intrinsic tribological behavior of a thin silicon oxide film. The results of the present study illustrate that significantly different friction properties can occur at different scales and provide new insight into frictional transitions commencing over a wide range of loads (or mean contact pressures) and apparent contact areas.

#### ACKNOWLEDGMENTS

This research was funded by the Director, Office of Energy Research, Office of Basic Energy Sciences, Materials Sciences Division, of the U.S. Department of Energy under Contract No. DE-AC0376SF00098. The authors would like to acknowledge W. Lu for assistance in the use of the SFM

and the Materials Department of ETH, Switzerland, for the scholarship awarded to partially support the studies of the first author at the University of California at Berkeley.

- <sup>1</sup>X. Xiao, J. Hu, D. H. Charych, and M. Salmeron, *Langmuir* **12**, 235 (1996).
- <sup>2</sup>J.-B. D. Green, M. T. McDermott, M. D. Porter, and L. M. Siperko, *J. Phys. Chem.* **99**, 10960 (1995).
- <sup>3</sup>H. Schönherr and G. J. Vancso, *Macromolecules* **30**, 6391 (1997).
- <sup>4</sup>B. Wei and K. Komvopoulos, *J. Tribol.* **119**, 823 (1997).
- <sup>5</sup>W. Lu and K. Komvopoulos, *J. Appl. Phys.* **85**, 2642 (1999).
- <sup>6</sup>K. Komvopoulos, N. Saka, and N. P. Suh, *J. Tribol.* **107**, 452 (1985).
- <sup>7</sup>P. F. Smith, R. Nisman, C. Ng, and G. J. Vancso, *Polym. Bull.* **33**, 459 (1994).
- <sup>8</sup>H. Yelle, H. Benabdallah, and H. Richards, *Wear* **149**, 341 (1991).
- <sup>9</sup>T. S. Barrett, G. W. Stachowiak, and A. W. Batchelor, *Wear* **153**, 331 (1992).
- <sup>10</sup>M. A. Spalding and K. S. Hyun, *Polym. Eng. Sci.* **35**, 557 (1995).
- <sup>11</sup>Q. Wang, X. Kong, L. Zhu, J. Zhe, and Y. Fan, *J. Appl. Polym. Sci.* **58**, 903 (1995).
- <sup>12</sup>L. Lavielle, *Wear* **157**, 181 (1992).
- <sup>13</sup>K. Komvopoulos, N. Saka, and N. P. Suh, *J. Tribol.* **108**, 301 (1986).
- <sup>14</sup>N. P. Suh, *Tribophysics* (Prentice-Hall, Englewood Cliffs, NJ, 1986).
- <sup>15</sup>D. H. Gracias and G. A. Somorjai, *Macromolecules* **31**, 1269 (1998).
- <sup>16</sup>D. F. Ogletree, R. W. Carpick, and M. Salmeron, *Rev. Sci. Instrum.* **67**, 3298 (1996).
- <sup>17</sup>K. L. Johnson, *Contact Mechanics* (Cambridge University Press, New York, NY, 1987).
- <sup>18</sup>S. Rose, *Fundamental Principles of Polymeric Materials*, 2nd ed (Wiley, New York, NY, 1999), p. 45.
- <sup>19</sup>C. G'Sell, B. Paysant-Le Roux, A. Dahoun, C. Cunat, J. von Stebut, and D. Mainard, *Tenth International Conference on Deformation, Yield and Fracture of Polymers* (The Institute of Materials, London, 1997), pp. 57–60.
- <sup>20</sup>C. Klapperich, K. Komvopoulos, and L. Pruitt, *J. Tribol.* **121**, 394 (1999).